Cyclotron motion in a microwave cavity: Lifetime and frequency shifts

Lowell S. Brown, Gerald Gabrielse, Kristian Helmerson, and Joseph Tan
Department of Physics, FM-15, University of Washington, Seattle, Washington 98195
(Received 13 May 1985)

The interaction of a bound electron with the radiation field produced by the image charges that represent a surrounding cavity produces a shift in its orbital frequency and in its radiative decay time. We calculate the frequency shift and the change in the damping constant for a cyclotron motion at the midpoint of a lossy, cylindrical cavity. A change in the cyclotron damping constant has, in fact, been observed in the University of Washington $g-2$ experiments. These experiments employ electrodes with a hyperbolic shape, but our calculable model should give a useful indication of the size of the effects for them. The frequency shift can easily be so large as to have important consequences for the $g-2$ measurements, and this systematic effect warrants a thorough experimental investigation. As an intermediate step in this calculation, we also compute the corresponding alterations for a charged particle in the midplane between two infinite parallel conductors.

I. INTRODUCTION

A charge accelerated in free space emits electromagnetic radiation. The radiation can be substantially modified, however, when the accelerated charge is within a conducting cavity, as pointed out long ago.[1] The radiation of a cyclotron motion can be strongly enhanced when the cyclotron frequency coincides with the frequency of an appropriate eigenmode of the cavity. Resonant cavities are often used in lasers to take advantage of the analogous phenomenon. On the other hand, the radiation can be inhibited when the cyclotron frequency is near no cavity mode to which it can couple.

Until recently, such inhibition of the radiation had not been observed, though experiments to do so with Rydberg atoms have been suggested[2] and are now underway. The first observation of inhibited radiation within a cavity, in fact, took place with a cyclotron oscillator.[3] The cyclotron motion of a single electron, within the cavity formed by the electrodes of a Penning trap, was observed to have a radiative damping rate which was longer than that occurring in free space. In addition, the damping rate was observed to change as the cyclotron frequency was changed, with the cavity left unchanged: The radiative damping time changed from 4 times longer than the free-space value to a value shorter than the free-space value. A later confirming observation of inhibited radiation in a different trap indicated a damping time nearly 10 times longer than the value for free space.[4]

The lengthening of the cyclotron damping time is very important for the precision measurements of the electron and positron cyclotron frequencies which are done within Penning traps. The favorable feature of the lengthened damping time is that it corresponds to a reduced cyclotron linewidth, making possible, in principle, a higher-precision measurement of the cyclotron frequency. On the other hand, if the couplings between the cyclotron oscillator and the oscillators which represents the cavity modes can cause a change in the damping rate, they can also cause a shift in the cyclotron oscillation frequency. Cavity-induced shifts in the cyclotron frequency are extremely undesirable for precision measurements and are a principle focus of this work. To assess the accuracy needed in the theoretical formula which relates the observed cyclotron frequency $\bar{\omega}_c$ to the cyclotron frequency ω_c in the absence of the cavity, we note that the measured anomaly is expressed as

$$a=\frac{g-2}{2}=\frac{\omega_s-\omega_c}{\omega_c}\ , \tag{1.1}$$

where ω_s is the spin precession frequency. Thus if the cavity frequency shift

$$\Delta\omega_c=\bar{\omega}_c-\omega_c \tag{1.2}$$

is not accounted for, it leads to a systematic error in the anomaly given by

$$\frac{\Delta a}{a}=\frac{1}{a}\frac{\Delta\omega_c}{\omega_c}\ . \tag{1.3}$$

Since the present precision[4] in the anomaly is $\Delta a/a\approx 4\times 10^{-9}$ and $a\approx 1.2\times 10^{-3}$, we see that the current experimental precision is upset if the cavity shift is larger than $\Delta\omega_c/\omega_c\approx 5\times 10^{-12}$. A previous estimate[5] suggested that the cavity shift could be of about this size. Our work shows that the situation may well be much more serious.

The hyperbolic shape of the electrodes used in the experiments, along with holes and slits in the electrodes, makes it difficult to calculate the mode structure in these traps. The mode structure of a cylindrical cavity, however, is well known. With this in mind, the possibility of producing an electrostatic quadrupole potential with cylindrical electrodes, which is of high enough quality to allow trapping and monitoring a single particle, is being investigated.[6] We accordingly calculate the interaction of a cyclotron oscillator with a cylindrical cavity, with the cyclotron orbit located at the center of the cavity. This detailed calculation provides, however, a useful indication of the properties of cyclotron motion in a hyperbolic cavity as well.

The basic outline of the calculation is described in Sec. II. The cyclotron motion gives a current which excites the cavity modes. These cavity fields in turn act back

upon the motion. In solving this coupled system a renormalization is required to avoid the infinities associated with self-energies. To do this, we solve first the problem of a cyclotron oscillator located between infinite parallel plates in Sec. III and then consider the cylindrical cavity in Sec. IV. By properly subtracting the parallel-plate contributions from the cavity contributions we avoid the infinities. Both Sec. III and Sec. IV are divided into a part A, which contains the necessary mathematical details, and a part B, which summarizes the results. An effort has been made to make it possible to skip Secs. III A and IV A if the details are not required. The radiative damping widths and the corresponding shifts in the cyclotron frequency are calculated as a function of the cyclotron frequency. Both depend upon the quality factor Q of the cavity, which has been included in an approximate but sufficiently accurate fashion. In the frequency range which corresponds to that being used for the precision measurements, a Q value of 1000 yields a damping time which can be as much as 10 times longer than that in free space. At the same time, the fractional frequency shift can be as large as 90×10^{-12} which substantially exceeds the present experimental accuracy which corresponds to a shift of 5×10^{-12}. For higher Q values the shifts can be even larger. We should point out that the present accuracy in the theoretical value for the anomaly, including the uncertainty in the fine-structure constant, is given by[7] $\Delta a/a\approx140\times10^{-9}$. Hence a frequency shift as large as $\Delta\omega_c/\omega_c\approx140\times10^{-12}$ would not be revealed by comparing the experimental and theoretical values for the anomaly.

Finally, we point out that while the frequency shifts we calculate here affect the accuracy of the measurements of the electron and positron magnetic moments, these shifts are entirely different from recent claims[8,9] of direct cavity shifts in the spin magnetic moment of order 10^{-12}. These claims led to a demonstration[5] that the exact apparatus of quantum electrodynamics reduces to the classical theory used in this paper with no measurable shift in the spin magnetic moment. The work of Ref. 5 also indicates how our results can be extended to atomic systems. This may be of interest for experiments presently in progress.[2] A brief account of the present work has been published.[10]

II. GENERAL FORMULATION

We are considering the classical motion of a charged particle which is bound in the typical field configuration of a Penning trap: a strong uniform magnetic field aligned along the z axis superimposed over a weak electrostatic potential. Such a field configuration gives rise to the free-space equation of motion

$$\dot{\mathbf{v}}-\boldsymbol{\omega}_c\times\mathbf{v}+\frac{e}{m}\nabla V(\mathbf{r})+\tfrac{1}{2}\gamma_c\mathbf{v}=\mathbf{0}\ , \tag{2.1}$$

where $\boldsymbol{\omega}_c$ is the cyclotron frequency of the particle's rotation in the magnetic field alone. The inclusion of the electrostatic potential $V(\mathbf{r})$ adds only very small accelerations to this fast motion, and so it suffices to take the damping constant to be that of a cyclotron circle,

$$\gamma_c(\omega_c)=4e^2\omega_c^2/3mc^3\ . \tag{2.2}$$

Our interest is in the modifications of this motion when it takes place about the center of an axially symmetric conducting cavity, with the orbit size a very small in comparison to the size d of the cavity. Neglecting insignificant image magnetic forces, the presence of the surrounding metallic cavity alters of the charged-particle equation of motion to read

$$\dot{\mathbf{v}}-\boldsymbol{\omega}_c\times\mathbf{v}+\frac{e}{m}\nabla V(\mathbf{r})+\tfrac{1}{2}\gamma_c\mathbf{v}=\frac{e}{m}\mathbf{E}'(\mathbf{r})\ . \tag{2.3}$$

Here $\mathbf{E}'(\mathbf{r})$ is the electric field at the position $\mathbf{r}(t)$ of the charged particle which is produced by the effective image charges that represent the cavity walls. It is the electric field acting on the particle omitting the trap field $[-\nabla V(\mathbf{r})]$ and also excluding the proper field of the particle itself. This proper field is accounted for by using the observed (free-space) electron mass m and by employing the free-space damping constant γ_c. It is convenient to split the field $\mathbf{E}'$ into longitudinal and transverse parts,

$$\mathbf{E}'={}^{(L)}\mathbf{E}'+{}^{(T)}\mathbf{E}'\ . \tag{2.4}$$

The longitudinal part ${}^{(L)}\mathbf{E}'$ is the gradient of the radiation-gauge scalar potential, while the transverse part ${}^{(T)}\mathbf{E}'$ is the time derivative of the radiation gauge vector potential. As we shall soon see, the major effect of ${}^{(L)}\mathbf{E}'$ is to alter the electrostatic binding field by an insignificant amount (in agreement with a previous estimate[11]), while it is the effect of ${}^{(T)}\mathbf{E}'$, which corresponds to the effects of the dynamical cavity modes, that can have significant consequences.

The longitudinal piece ${}^{(L)}\mathbf{E}'$ is obtained from the alteration brought about by the cavity on the static scalar potential produced by the charged particle. Thus

$${}^{(L)}\mathbf{E}'(\mathbf{r})=-\nabla e\mathscr{D}'(\mathbf{r},\mathbf{r}')\,|_{\mathbf{r}'=\mathbf{r}}\ . \tag{2.5}$$

Here $\mathscr{D}'(\mathbf{r},\mathbf{r}')$ is a solution to the homogeneous Laplace equation. Adding to it the free-space Green's function $1/|\mathbf{r}-\mathbf{r}'|$ produces the Coulomb Green's function appropriate to the cavity, a function which vanishes when either $\mathbf{r}$ or $\mathbf{r}'$ lies on the cavity surface. Since the charged particle moves about a small orbit near the center of the cavity, the first nontrivial term in the power-series expansion of ${}^{(L)}\mathbf{E}'(\mathbf{r})$ about $\mathbf{r}=\mathbf{0}$ suffices. The symmetry of the cavity gives ${}^{(L)}\mathbf{E}'(\mathbf{0})=\mathbf{0}$. Small imperfections make ${}^{(L)}\mathbf{E}'(\mathbf{0})$ nonvanishing, but this very small constant electric field is canceled by a very small shift in the equilibrium position of the trapping potential. Thus the first nontrivial term is a linear one,

$$\frac{e}{m}{}^{(L)}E'_k(\mathbf{r})=\sum_{l=1}^{3}\Omega_{kl}r_l\ , \tag{2.6}$$

where

$$\Omega_{kl}=-\frac{e^2}{m}[\nabla_k\nabla_l\mathscr{D}'(\mathbf{r},\mathbf{r}')\,|_{\mathbf{r}'=\mathbf{r}}+\nabla_k\nabla'_l\mathscr{D}'(\mathbf{r},\mathbf{r}')\,|_{\mathbf{r}'=\mathbf{r}}]\ . \tag{2.7}$$

The first term in the square brackets is symmetrical in the vector indices k,l and traceless since $\mathscr{D}'(\mathbf{r},\mathbf{r}')$ obeys the Laplace equation. Moreover, this term shares the axial symmetry of the trapping potential. Hence its effect is absorbed by a small redefinition of this potential. Since the Green's function is symmetric,

$$\mathscr{D}'(\mathbf{r},\mathbf{r}')=\mathscr{D}'(\mathbf{r}',\mathbf{r}) , \tag{2.8}$$

the second term in the square brackets is symmetrical in the vector indicies k,l. This second term also has axial symmetry, but it is not traceless. The scalar part

$$\bar{\Omega}_{kl}=\delta_{kl}\Omega , \tag{2.9}$$

$$\Omega=\tfrac{1}{3}\sum_{m=1}^{3}\Omega_{mm} , \tag{2.10}$$

cannot be absorbed by a redefinition of the trapping potential. The correction is, however, very small: The double gradient of $\mathscr{D}'(\mathbf{r},\mathbf{r}')$ is of order $1/d^3$, where d is the characteristic trap size. Hence

$$\Omega\approx\frac{e^2}{md^3}=\frac{a_0}{d}\frac{e^2}{a_0}\frac{1}{md^2} . \tag{2.11}$$

Here we have introduced the Bohr radius $a_0\approx 5\times 10^{-9}$ cm since the binding energy of the hydrogen atom $e^2/2a_0\simeq 14$ eV is about e times a typical trapping voltage V_0 (a voltage produced by batteries). Therefore

$$\Omega\approx\frac{a_0}{d}\frac{eV_0}{md^2} , \tag{2.12}$$

and we see that this correction is of order $a_0/d\approx 10^{-8}$ relative to the strength of the trapping potential. Since this is an entirely negligible correction, a more elaborate evaluation is not necessary, and we turn to the potentially important effects of the transverse electric field.

The transverse electric field may be expressed as the time derivative of a vector potential and thus as

$${}^{(T)}E_k'(t,\mathbf{r})=-\frac{\partial}{\partial t}\int dt'\sum_{l=1}^{3}D_{kl}'(t-t';\mathbf{r},\mathbf{r}(t'))ev_l(t')/c^2 . \tag{2.13}$$

Here $D_{kl}'(t-t';\mathbf{r},\mathbf{r}')$ is the retarded, transverse, radiation gauge Green's-function alteration brought about by the cavity. Adding it to the free-space Green's function produces the full Green's function which obeys the relevant boundary conditions on the cavity walls. Since the charged particle is confined to a small region near the center of the cavity, it suffices to set $\mathbf{r}(t)=\mathbf{0}=\mathbf{r}(t')$ in Eq. (2.13). Only the fast cyclotron motion has any significant correction from this field. Adopting complex coordinates and Fourier transforming according to

$$v(t)=v_x(t)-iv_y(t)\sim e^{-i\omega t} \tag{2.14}$$

with

$$D_{kl}'(t-t';\mathbf{r},\mathbf{r}')=\int\frac{d\omega}{2\pi}e^{-i\omega(t-t')}\tilde{D}_{kl}'(\omega;\mathbf{r},\mathbf{r}') , \tag{2.15}$$

one finds that inserting the field (2.13) into the equation of motion (2.3) yields the condition

$$\omega-\omega_c'+i\gamma_c/2=-\omega r_0\tilde{D}_{xx}'(\omega;0,0) , \tag{2.16}$$

where $r_0=e^2/mc^2\approx 3\times 10^{-13}$ cm is the classical electron radius. The effect of the trapping potential is to replace the cyclotron frequency ω_c by a slightly modified frequency[12] ω_c' which appears on the left-hand side of Eq. (2.16). The simplicity of the right-hand side of Eq. (2.16) results from the axial symmetry which implies that $\tilde{D}'(\omega;0,0)$ is proportional to the unit dyadic in the x-y plane, with the proportionality constant $\tilde{D}_{xx}'(\omega;0,0)=\tilde{D}_{yy}'(\omega;0,0)$.

In general, the Green's-function modification $\tilde{D}_{xx}'(\omega;0,0)$ is a complex number and thus the presence of the cavity modifies the cyclotron decay constant away from its free-space value γ_c as well as altering the resonance frequency away from ω_c'. In the limit of a perfect cavity with perfectly conducting walls, the imaginary part of $\tilde{D}_{xx}'(\omega;0,0)$ cancels γ_c exactly. In this limit there is no decay of the cyclotron motion because there is no dissipative process to absorb the energy.

To assess the size of the correction to the cyclotron frequency given by the right-hand side of Eq. (2.16), we note that simple dimensional analysis informs us that

$$\tilde{D}_{xx}'(\omega;0,0)=F(\omega d/c)/d , \tag{2.17}$$

where F is a dimensionless function of the dimensionless ratio $\omega d/c=d/\lambda\!\!\!^{-}$. This function describes the retarded propagation of the radiation field emitted by the motion of the image charges that represent the cavity walls, and thus one expects that $F(\omega d/c)$ will be roughly of the order of unity even for a large argument. Using the typical values for a Penning trap $r_0/d\approx 1\times 10^{-12}$ and $\omega d/c\approx 10$, and taking $F(\omega d/c)\approx 1$, we see that the correction to the cyclotron frequency is roughly on the order of one part in 10^{12}, which is almost as large as the current precision of the geonium experiments.[4] Moreover, since $\gamma_c/\omega_c\sim 10^{-13}$, we also see that the damping constant may be significantly altered. Clearly this effect warrants a more careful examination, to which we now turn.

Before passing to the quantitative treatment, some qualitative, clarifying remarks are in order. We first ignore the renormalization problem so that the Green's-function correction $\tilde{D}_{xx}'(\omega;0,0)$ on the right-hand side of Eq. (2.16) is replaced by the full Green's function and the decay constant γ_c is omitted on the left-hand side. In this case we may express the Green's function by a mode sum to obtain

$$\omega-\omega_c'=\omega\sum_N\frac{\lambda_N^2}{\omega^2+i\omega\Gamma_N-\omega_N^2} . \tag{2.18}$$

Here ω_N is the eigenfrequency of the Nth mode and Γ_N is the decay constant of this mode with $Q_N=\omega_N/\Gamma_N$ the corresponding quality factor of the mode. The coupling constant λ_N^2 in the numerator is related to the square of a wave function, and so it is a positive number, while the sign of the damping term $+i\omega\Gamma_N$ in the denominator is dictated by the causal requirement of decay rather than growth in time. The formula (2.18) expresses the frequency shift of the cyclotron motion, which is essentially harmonic, in terms of its interaction with the infinite number of cavity modes of the radiation field, each of whose amplitudes is a harmonic oscillator. Thus formula (2.18) represents the cyclotron frequency shift in terms of the solution of an (infinite) set of coupled harmonic oscillators. A simple dimensional argument shows that λ_N^2 is of order $r_0/d^3c^2\sim(r_0/d)\omega_N^2$. Therefore, away from any cavity resonance $\omega=\omega_N$, we have a small frequency shift of the order $(\omega-\omega_c')/\omega\sim r_0/d$, in agreement with our previous estimate. However, near a cavity resonance, we

can have a frequency shift (from this one mode) as large as $(\omega-\omega_c')/\omega\sim\pm(r_0/d)(\omega_N/\Gamma_N)=\pm(r_0/d)Q_N$, which is much larger. This frequency shift disappears exactly on resonance, but in this case there is a large change in the cyclotron decay constant of order $(r_0/d)Q_N\omega\sim\gamma_c Q_N$. (In these last two estimates we have neglected purely numerical factors which may be fairly large.)

The story we have just told suffers from a serious omission, the omission of the necessity of a renormalization. Replacing the cavity walls with an absorbing material and taking the limit of an infinitely large cavity must yield the free-space limit. In this limit, the imaginary part of the right-hand side of Eq. (2.18), the absorptive contribution, must reproduce the free-space decay constant $-i\gamma_c/2$. But in this limit, the real part of the right-hand side of Eq. (2.18) is infinite since it contains the reactive effect of the proper field of the charged particle. Clearly, this divergence also appears in the original cavity configuration. As is well known, this infinity is correctly dealt with by removing the free-space reactive contribution of the charged particle's proper field and employing the observed free-space value of the charged particle's mass. Thus the formal mode sum in Eq. (2.18) diverges, and it must be renormalized by subtracting out the real part of the free-space limit. Since this is a delicate operation, we shall instead return to the previous formula (2.16) which expresses the (complex) frequency shift in terms of the alteration $\tilde{D}'_{xx}(\omega;0,0)$ of the Green's function brought about by the presence of the cavity.

To have a tractable problem, but one which is of direct experimental interest,[6] we shall consider a right-cylindrical cavity as illustrated in Fig. 1. We shall at first neglect dissipation and treat the cavity walls as perfect conductors. We shall later take account of dissipation by replacing the individual cavity widths Γ_N with an average value Γ. Referring to the (formal) mode sum (2.18), we see that since $\Gamma^2\ll\omega_N^2$, this is tantamount to replacing the frequency ω by the complex number $\omega+i\Gamma/2$. To unambiguously determine the renormalized alteration $\tilde{D}'_{xx}(\omega;0,0)$, we note that the limit in which the cavity radius R is taken to infinity with the cylindrical side replaced with an absorbing material yields a geometry with two parallel, infinite perfectly conducting planes a distance $2L$ apart. Thus we express the Green's function as the sum of the Green's function for the parallel-plate problem plus the solution to the homogeneous wave equation which corrects for the presence of the cylindrical wall. Since the Green's function for the two-parallel-plate geometry can be expressed as an infinite sum of image contributions,[13] the removal of the proper field term is now trivial: one simply omits the direct contribution from the sum.

We solve the simple parallel-plate problem in Sec. III. This problem is of some interest in its own right. We then go on to solve the cylindrical-cavity problem in Sec. IV.

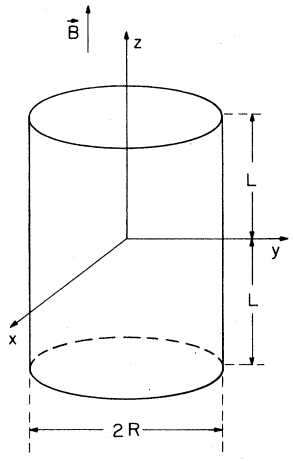

FIG. 1. Cylindrical cavity of radius R and length $2L$, with its symmetry axis along the z axis and its center at the origin of the coordinate system. There is a uniform magnetic field $\mathbf{B}$ in the z direction, and the charged particle moves in a small orbit about this field near the center.

III. PARALLEL PLATES

Here we work out the (complex) shift in the cyclotron frequency for a charged particle moving in the midplane between two infinite parallel plates a distance $2L$ apart as shown in Fig. 2. First we shall treat the plates as perfectly conducting planes. Later on the dissipative effects of plates with finite conductivity will be taken into account.

A. Calculation

First off, let us recall that, within a general conducting cavity, the Green's function for the radiation gauge vector potential obeys

$$\left[-\nabla^2-\frac{\omega^2}{c^2}\right]\tilde{D}_{kl}(\omega;\mathbf{r}-\mathbf{r}')=4\pi\left[1-\nabla\frac{1}{\nabla^2}\nabla\right]_{kl}\delta(\mathbf{r}-\mathbf{r}')\ . \tag{3.1}$$

We shall often represent the Coulomb Green's function by an operator shorthand notation as used here,

$$\mathscr{D}(\mathbf{r},\mathbf{r}')=\frac{1}{-\nabla^2}\delta(\mathbf{r}-\mathbf{r}')\ . \tag{3.2}$$

One must keep in mind, however, that $\mathscr{D}(\mathbf{r},\mathbf{r}')$ is defined so as to vanish when either $\mathbf{r}$ or $\mathbf{r}'$ lies on a cavity wall.

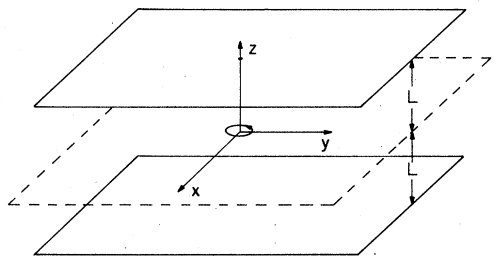

FIG. 2. Two infinite parallel conducting plates at $z=L$ and $-L$. Small circle in the midplane ($z=0$) centered at the origin of the coordinate system represents the trajectory of the electron under a uniform magnetic field aligned along the z axis.

These boundary conditions must be used so as to ensure that the tangential components of the radiation gauge Green's function vanish on a cavity wall.

The free-space Green's function has the familiar, Fourier-transform construction

$$\tilde{D}^{(0)}_{kl}(\omega;\mathbf{r}-\mathbf{r}') = 4\pi \int \frac{d^3k}{(2\pi)^3}\left[\delta_{kl}-\frac{k_k k_l}{k^2}\right]\frac{e^{i\mathbf{k}\cdot(\mathbf{r}-\mathbf{r}')}}{k^2-(\omega+i\epsilon)^2/c^2} . \tag{3.3}$$

Here the $\epsilon\to 0+$ defines the frequency contour integration which produces a causal, retarded response in time. The Green's function for a single conducting plate is obtained by simply adding a single image function to Eq. (3.3). This image construction which is familiar in the electrostatic case generalizes to the full electromagnetic field since the retardation times to the plate from the charge and its image are identical. For the case of two parallel plates, the solution can be expressed in terms of an infinite set of images as shown in Fig. 3. This again is the same as the familiar electrostatic construction. Thus we obtain

$$\tilde{D}_{xx}(\omega;0,0)=\sum_{n=-\infty}^{+\infty}(-1)^n F(2nL) , \tag{3.4}$$

in which

$$F(z)=4\pi\int\frac{d^3k}{(2\pi)^3}\left[1-\frac{k_x^2}{k^2}\right]\frac{e^{-ik_z z}}{k^2-(\omega+i\epsilon)^2/c^2} . \tag{3.5}$$

The integrations involved in this Fourier transform are elementary, and they give

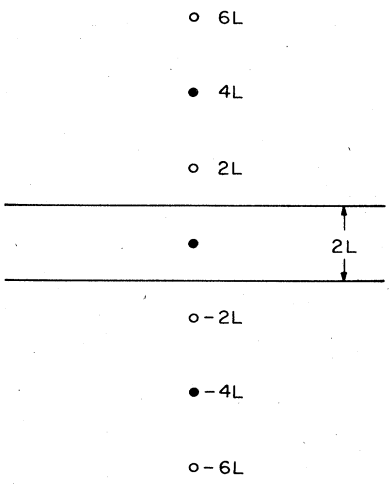

FIG. 3. Illustration of image charges induced by an electron in the midplane of the parallel-plate configuration shown in Fig. 2. This infinite set of images alternating in sign and regularly spaced by a distance $2L$ is used in the construction of the Green's-function alteration caused by the two plates.

$$F(z)=\frac{1}{|z|}\left[e^{i\omega|z|/c}\left[1+\frac{ic}{\omega|z|}-\frac{c^2}{(\omega z)^2}\right]+\frac{c^2}{(\omega z)^2}\right] . \tag{3.6}$$

The Green's-function alteration caused by the two plates—the Green's function with the self-interaction contribution removed—is simply obtained by deleting the $n=0$ term in the sum (3.4). Since $F(z)$ is an even function, we have

$$\tilde{D}'_{xx}(\omega;0,0)=2\sum_{n=1}^{\infty}(-1)^n F(2nL) . \tag{3.7}$$

The sum entails the functions

$$C_p(x)=-2\sum_{n=1}^{\infty}\frac{(-1)^n}{n^p}\cos(nx) \tag{3.8a}$$

and

$$S_p(x)=-2\sum_{n=1}^{\infty}\frac{(-1)^n}{n^p}\sin(nx) \tag{3.8b}$$

for $p=1,2,3$. By writing the cosine and sine in Eqs. (3.8) in terms of exponentials it is easy to see that the sums for $p=1$ are elementary. It is straightforward to compute

$$C_1(x)=\ln[4\cos^2(x/2)] . \tag{3.9a}$$

The computation of $S_1(x)$ is a bit tricky because one must be careful to get the right branch of a logarithm. Bearing in mind that $S_1(0)=0$ and that $S_1(x)$ is periodic with period 2π, one finds that

$$S_1(x)=x-2\pi\left[\frac{x}{2\pi}+\frac{1}{2}\right] , \tag{3.9b}$$

where $[y]$ denotes the integer part of y. The curve of $S_1(x)$ versus x is of a sawtooth form, with the sign of $S_1(x)$ flipping when x passes through an odd integer number of π's. The sums for $p=2$ and 3 may be expressed in terms of integrals of $C_1(x)$ and $S_1(x)$ since it follows from Eqs. (3.8) that

$$\frac{d}{dx}C_p(x)=-S_{p-1}(x) \tag{3.10a}$$

and

$$\frac{d}{dx}S_p(x)=C_{p-1}(x) . \tag{3.10b}$$

In particular, noting that $C_2(0)=\zeta(2)=\pi^2/6$, one finds that

$$C_2(x)=\frac{\pi^2}{6}-\frac{1}{2}S_1(x)^2 \tag{3.11}$$

and then in turn, remembering that $S_3(0)=0$,

$$S_3(x)=\frac{\pi^2}{6}S_1(x)-\frac{1}{6}S_1(x)^3 . \tag{3.12}$$

B. Results

We have now solved the parallel-plate problem. Recalling Eqs. (2.16) and (2.2) we have

$$\omega-\omega_c'=-\frac{i}{2}\gamma_c(\omega)+\omega\Sigma_P(\omega)$$
$$=-\frac{i}{2}I_P(\omega)+R_P(\omega)\ , \tag{3.13}$$

where

$$\gamma_c(\omega)=\frac{4\omega^2 r_0}{3c} \tag{3.14}$$

and

$$\Sigma_P(\omega)=-r_0\tilde{D}'_{xx}(\omega;0,0)\ . \tag{3.15}$$

In the second line of Eq. (3.13) we have separated out the imaginary and real parts. Explicit forms for $I_P(\omega)$ and $R_P(\omega)$ follow from Eqs. (3.6)—(3.15) and a little arithmetic. They depend upon the dimensionless variable

$$\xi=\frac{\omega L}{\pi c}=\frac{2L}{\lambda} \tag{3.16}$$

which is the (fractional) number of wavelengths at frequency ω which fit between the plates. The forms are

$$I_P(\omega)=\gamma_c(\omega)\left[\frac{[\xi+\frac{1}{2}]^3}{4\xi^3}+\frac{3[\xi+\frac{1}{2}]}{4\xi}-\frac{[\xi+\frac{1}{2}]}{16\xi^3}\right] \tag{3.17}$$

and

$$R_P(\omega)=\omega\frac{r_0}{L}\left[\frac{1}{2}\ln[4\cos^2(\pi\xi)]+\frac{1}{2\pi\xi}\sum_{n=1}^{\infty}\frac{(-1)^n}{n^2}\sin(2\pi n\xi)+\frac{1}{(2\pi\xi)^2}\sum_{n=1}^{\infty}\frac{(-1)^n}{n^3}[\cos(2\pi n\xi)-1]\right]. \tag{3.18}$$

The decay constant $I_P(\omega)$ given by Eq. (3.17) is plotted in Fig. 4. With $\xi<\frac{1}{2}$, less than half a wavelength fits between the plates. In this case electromagnetic waves cannot propagate between the plates, the charged particle cannot radiate, and $I_P(\omega)=0$. The decay constant $I_P(\omega)$ jumps discontinuously to $3\gamma_c(\omega)$ and then decreases as ξ increases past $\xi=\frac{1}{2}$, which is the first threshold for propagating waves. Further discontinuous jumps take place as ξ passes through thresholds at odd half-integers. (There are no thresholds at the integers since there is a node at the midplane position of the charged particle when an even number of half-wavelengths fit between the two plates.) As ξ becomes large, there is no obstacle to the radiation of the charged particle, and $I_P(\omega)$ approaches the free-space value $\gamma_c(\omega)$.

The real part of the frequency shift given by Eq. (3.18) is sketched in Fig. 5. As illustrated in the figure, the eigenfrequencies ω are determined by the intersection of the line $y=\omega_c'-\omega$ and the curve $y=-R_P(\omega)$. Several roots appear if ω_c' is sufficiently large. This multiplicity of roots, however, is a consequence of the idealization which replaces a metallic plate by a perfectly conducting plane. This idealization gives rise to the singular logarithm in Eq. (3.18) which diverges when ξ is an odd half-integer. (For these values of ξ the retardation phase exactly cancels the alternating signs of the image charges and the resultant infinite image sum involves $1/n$ which diverges logarithmically.) Power flows into real physical plates rather than having a vanishing Poynting vector as in the perfect conductor idealization. This dissipative effect can be modeled by diminishing successive pairs of image charges by a constant ratio $e^{-\kappa}$ that is slightly less than unity, with the nth image charge modified by the factor $e^{-n\kappa}$. Since the ratio of the electromagnetic energy flux into a cavity wall to the energy density near the wall is approximately given by $\omega\delta$, where δ is the skin depth of the wall, we have roughly $\kappa\approx\omega\delta/c$. Referring back to Eqs. (3.6) and (3.7), we see that the dissipative effect can be simply modeled by the replacement

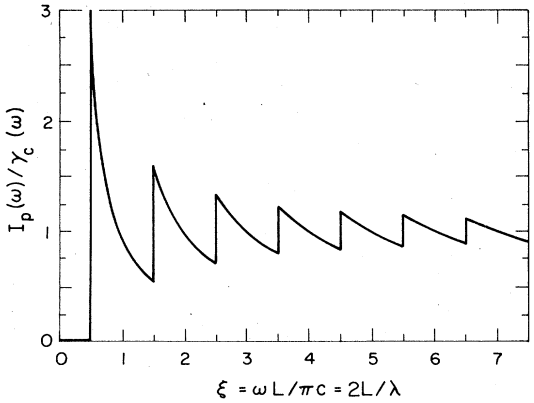

FIG. 4. The decay constant $I_P(\omega)/\gamma_c(\omega)$ given in Eq. (3.17) plotted against ξ, the number of wavelengths at frequency ω that fit between the parallel conducting plates.

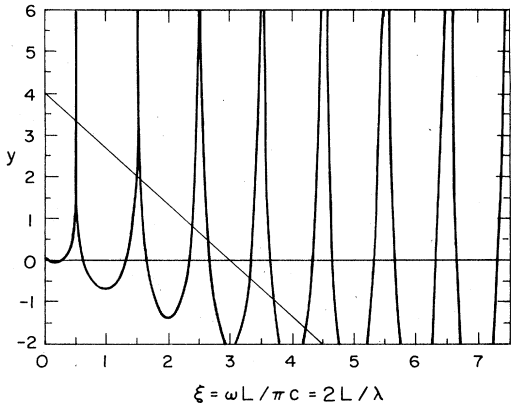

FIG. 5. A sketch for the real part of the frequency shift given in Eq. (3.18). The eigenfrequencies ω are determined by the intersections of the curve $y=-(L/r_0)(L/\pi c)R_P(\omega)$ and the line $y=(L/r_0)(\xi_c-\xi)$, where $\xi_c=\omega_c L/\pi c$. Cyclotron frequency was chosen so as to give $\xi_c=3$. In order to illustrate the multiple roots that appear when the line intersects the curve, an extreme ratio $L/r_0=\frac{4}{3}$ has been used.

$$\omega \rightarrow \omega + \frac{i}{2}\Gamma \tag{3.19}$$

in $\Sigma_P(\omega)$, where

$$\Gamma \approx \omega\delta/L \ . \tag{3.20}$$

With ω extended to a complex variable, the decomposition into imaginary and real parts displayed in Eqs. (3.17) and (3.18) is no longer useful. Instead, we simply use the complex form

$$\Sigma_P(\omega) = \frac{r_0}{L}\ln(1+e^{2i\omega L/c}) - \frac{r_0}{L}\sum_{n=1}^{\infty}(-1)^n\left[e^{2in\omega L/c}\left[\frac{ic}{2n^2L\omega} - \frac{c^2}{4n^3L^2\omega^2}\right] + \frac{c^2}{4n^3L^2\omega^2}\right] . \tag{3.21}$$

We now have

$$-\frac{i}{2}I_P(\omega) + R_P(\omega) = -\frac{i}{2}\gamma_c(\omega) + i\omega\,\mathrm{Im}\Sigma_P(\omega + i\Gamma/2) + \omega\,\mathrm{Re}\Sigma_P(\omega + i\Gamma/2) \ . \tag{3.22}$$

In Fig. 6 we plot the modified $R_P(\omega)$, taking $\delta/L = 2\times10^{-3}$. Since the frequency shift is now always very small, it is simply given by $R_P(\omega_c')$. Note that this shift vanishes at two points between successive odd half-integer values of ξ, while $R_P(\omega_c')L/\omega r_0$ approaches $\frac{1}{2}\ln 2$ when $\omega \rightarrow 0$ and vanishes when $\omega \rightarrow \infty$. The modified decay constant $I_P(\omega)$ is altered only slightly from the ideal limit with no cavity dissipation shown in Fig. 4: The sharp discontinuities in $I_P(\omega)$ are smoothed and $I_P(\omega)$ now has a very small but nonvanishing contribution below the first threshold $\xi = \frac{1}{2}$. Since with $\delta/L = 2\times10^{-3}$ these alterations are hardly visible on the scale of Fig. 4, and we do not give a separate plot of $I_P(\omega)$ including the effects of cavity dissipation.

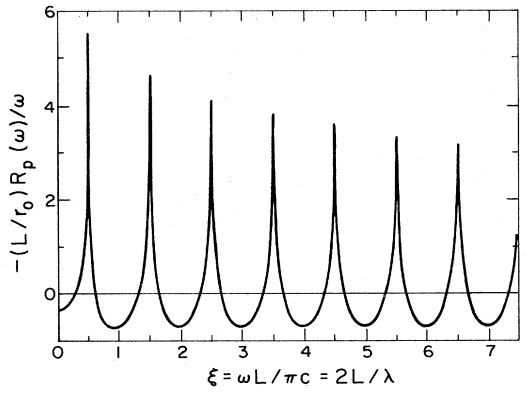

FIG. 6. Plot of $-(L/\omega r_0)R_P(\omega)$ vs ξ given by Eqs. (3.18) and (3.22) for dissipative plates with $\delta/L = 2\times10^{-3}$. Note that the multiple roots no longer appear.

IV. CYLINDRICAL CAVITY

We turn now to the problem which is our major interest, the frequency shift and modification of the decay rate for a small cyclotron orbit bound to the center of a cylindrical cavity as illustrated in Fig. 1. We denote the radius of the cavity by R, the length by $2L$, and use a coordinate frame whose z axis lies along the axis of circular symmetry and whose origin is at the center of the cavity. Again we shall first work with a perfectly conducting cavity and later generalize to a dissipative cavity whose walls have a finite conductivity.

A. Calculation

To construct the radiation gauge Green's function $\tilde{D}_{kl}(\omega;\mathbf{r},\mathbf{r}')$ for the cavity, we define

$$\nabla_\perp^2 = \nabla^2 - \frac{\partial^2}{\partial z^2} \ , \tag{4.1}$$

and note the formal operator identity

$$(\nabla\times\hat{\mathbf{z}})_k\frac{1}{\nabla_\perp^2}(\nabla\times\hat{\mathbf{z}})_l + [\nabla\times(\nabla\times\hat{\mathbf{z}})]_k\frac{1}{\nabla^2\nabla_\perp^2}[\nabla\times(\nabla\times\hat{\mathbf{z}})]_l = \left[1 - \nabla\frac{1}{\nabla^2}\nabla\right]_{kl} . \tag{4.2}$$

This identity enables us to express the tensor Green's function $\tilde{D}_{kl}(\omega;\mathbf{r},\mathbf{r}')$ in terms of scalar functions $G_E(\omega;\mathbf{r},\mathbf{r}')$ and $G_M(\omega;\mathbf{r},\mathbf{r}')$ that correspond to the TE and TM decomposition of the cavity modes. Using $\overleftarrow{\nabla}'$ to denote a gradient acting to the left on $\mathbf{r}'$ and writing

$$\tilde{D}_{kl}(\omega;\mathbf{r},\mathbf{r}') = (\nabla\times\hat{\mathbf{z}})_k\frac{1}{-\nabla_\perp^2}4\pi G_E(\omega;\mathbf{r},\mathbf{r}')(\overleftarrow{\nabla}'\times\hat{\mathbf{z}})_l + [\nabla\times(\nabla\times\hat{\mathbf{z}})]_k\frac{1}{\nabla^2\nabla_\perp^2}4\pi G_M(\omega;\mathbf{r},\mathbf{r}') \times[\overleftarrow{\nabla}'\times(\overleftarrow{\nabla}'\times\hat{\mathbf{z}})]_l \ , \tag{4.3}$$

one finds, using naive operator manipulations neglecting operator ordering, that the Green's-function equation (3.1) is obeyed if G_E and G_M satisfy

$$(-\nabla^2 - \omega^2/c^2)G_{E,M}(\omega;\mathbf{r},\mathbf{r}') = \delta(\mathbf{r}-\mathbf{r}') \ . \tag{4.4}$$

We shall show below that this result of naive manipulation is also obtained by a careful treatment. The boundary condition that the tangential components of the electric field vanish on the cavity surface S requires that $\tilde{D}_{kl}(\omega;\mathbf{r},\mathbf{r}')$ vanish when $\mathbf{r}$ is at a point on S and k is a component along S or when $\mathbf{r}'$ is at a point on S and l is a component along S. Examining Eq. (4.3), one sees that the boundary condition requires that $G_E(\omega;\mathbf{r},\mathbf{r}')$ must vanish when $\mathbf{r}$ or $\mathbf{r}'$ lies on the two end planes of the cavity while its normal gradient must vanish when $\mathbf{r}$ or $\mathbf{r}'$ lies on the cylindrical surface. Conversely, the boundary condition requires that $G_M(\omega;\mathbf{r},\mathbf{r}')$ must vanish when $\mathbf{r}$ or $\mathbf{r}'$ lies on the cylindrical surface with its normal gradient vanishing when $\mathbf{r}$ or $\mathbf{r}'$ lies on the two end planes.

We employ cylindrical coordinates and construct the

scalar Green's functions by the infinite series

$$G(\omega;\mathbf{r},\mathbf{r}')=\sum_{n=0}^{\infty}\frac{1}{L}t(k_nz)t(k_nz')\mathcal{G}(\mu_n;\boldsymbol{\rho},\boldsymbol{\rho}') . \tag{4.5}$$

Here $t(k_nz)$ is a sine or cosine obeying

$$\left[\frac{d^2}{dz^2}+k_n^2\right]t(k_nz)=0 . \tag{4.6}$$

with the wave-number eigenvalues k_n determined by the boundary conditions

$$t_E(k_nL)=0, \quad \text{TE} \tag{4.7a}$$

$$t'_M(k_nL)=0, \quad \text{TM} \tag{4.7b}$$

where the prime denotes the derivative. It will prove convenient to adopt the convention

$$\frac{d}{dz}t_M(k_nz)=k_nt_E(k_nz) . \tag{4.8}$$

Since

$$\sum_{n=0}^{\infty}\frac{1}{L}t(k_nz)t(k_nz')=\delta(z-z') , \tag{4.9}$$

we have

$$(-\nabla_\perp^2+\mu_n^2)\mathcal{G}(\mu_n;\boldsymbol{\rho},\boldsymbol{\rho}')=\delta(\boldsymbol{\rho}-\boldsymbol{\rho}') , \tag{4.10}$$

where

$$\mu_n=(k_n^2-\omega^2/c^2)^{1/2} . \tag{4.11}$$

Since moreover

$$\sum_{m=-\infty}^{\infty}\frac{1}{2\pi}e^{im(\phi-\phi')}=\delta(\phi-\phi') , \tag{4.12}$$

we may express the two-dimensional Green's functions as

$$\mathcal{G}(\mu_n;\boldsymbol{\rho},\boldsymbol{\rho}')=\sum_{m=-\infty}^{\infty}\frac{1}{2\pi}e^{im(\phi-\phi')}\mathcal{G}_m(\mu_n;\rho,\rho') , \tag{4.13}$$

where

$$\left[-\frac{d^2}{d\rho^2}-\frac{1}{\rho}\frac{d}{d\rho}+\frac{m^2}{\rho^2}+\mu_n^2\right]\mathcal{G}_m(\mu_n;\rho,\rho')=\frac{1}{\rho}\delta(\rho-\rho') . \tag{4.14}$$

We shall first solve this radial equation in the low-frequency region where $\omega<\pi c/2L$. In this region all the μ_n are positive, real numbers, and waves cannot propagate in the radial direction. Thus the solutions to the homogeneous counterpart of the radial Green's-function equation (4.14) are the modified Bessel function $I_{|m|}(\mu_n\rho)$, which is regular at $\rho=0$, and the modified Hankel function $K_{|m|}(\mu_n\rho)$, which vanishes exponentially as $\rho\to\infty$. The boundary conditions on the cylindrical surface $\rho=R$ are obeyed by the functions

$$F^{(E)}_{|m|}(\mu_n\rho)=K_{|m|}(\mu_n\rho)-\frac{K'_{|m|}(\mu_nR)}{I'_{|m|}(\mu_nR)}I_{|m|}(\mu_n\rho), \quad \text{TE} \tag{4.15a}$$

and

$$F^{(M)}_{|m|}(\mu_n\rho)=K_{|m|}(\mu_n\rho)-\frac{K_{|m|}(\mu_nR)}{I_{|m|}(\mu_nR)}I_{|m|}(\mu_n\rho), \quad \text{TM} . \tag{4.15b}$$

In view of the Wronskian

$$I_{|m|}(\mu\rho)\frac{d}{d\rho}F^{(E,M)}_{|m|}(\mu\rho)-F^{(E,M)}_{|m|}(\mu\rho)\frac{d}{d\rho}I_{|m|}(\mu\rho)=-\frac{1}{\rho} , \tag{4.16}$$

we see that the solutions to the inhomogeneous radial Green's-function equation are given by

$$\mathcal{G}^{(E,M)}_m(\mu_n;\rho,\rho')=I_{|m|}(\mu_n\rho_<)F^{(E,M)}_{|m|}(\mu_n\rho_>) , \tag{4.17}$$

where $\rho_<$ and $\rho_>$ denote, respectively, the lesser and greater of ρ and ρ'.

Formal, abstract operator methods were used in the construction (4.3) of the tensor Green's function. We must now give an explicit realization of this construction and show that the Green's-function equation (3.1) is indeed obeyed. The action of the inverse Laplace operators in Eq. (4.3) must preserve the boundary conditions defining the scalar Green's functions $G_{E,M}$. Hence one must set

$$\frac{1}{-\nabla_\perp^2}G_E(\omega;\mathbf{r},\mathbf{r}')=\sum_{n=0}^{\infty}\frac{1}{L}t_E(k_nz)t_E(k_nz')\times\frac{1}{-\mu_n^2}[\mathcal{G}^{(E)}(\mu_n;\boldsymbol{\rho},\boldsymbol{\rho}')-\mathcal{G}^{(E)}(0;\mathbf{p},\mathbf{p}')] . \tag{4.18}$$

The right-hand side of this equation clearly obeys the correct boundary conditions, and acting upon it with $-\nabla_\perp^2$ produces $G_E(\omega;\mathbf{r},\mathbf{r}')$. Similarly,

$$\frac{1}{\nabla^2\nabla_\perp^2}G_M(\omega;\mathbf{r},\mathbf{r}')=\sum_{n=0}^{\infty}\frac{1}{L}t_M(k_nz)t_M(k_nz')\frac{c^2}{\omega^2}\left[\frac{1}{-\mu_n^2}[\mathcal{G}^{(M)}(\mu_n;\boldsymbol{\rho},\boldsymbol{\rho}')-\mathcal{G}^{(M)}(0;\boldsymbol{\rho},\boldsymbol{\rho}')]+\frac{1}{k_n^2}[\mathcal{G}^{(M)}(k_n;\boldsymbol{\rho},\boldsymbol{\rho}')-\mathcal{G}^{(M)}(0;\boldsymbol{\rho},\boldsymbol{\rho}')]\right] . \tag{4.19}$$

To establish that with these explicit forms we do solve the radiation gauge Green's-function equation (3.1), we first note that the Coulomb Green's function [Eq. (3.2)] has the explicit construction

$$\mathscr{D}(\mathbf{r},\mathbf{r}')=\sum_{n=0}^{\infty}\frac{1}{L}t_E(k_nz)t_E(k_nz')\mathscr{G}^{(M)}(k_n;\boldsymbol{\rho},\boldsymbol{\rho}') \ . \tag{4.20}$$

Note that this construction obeys the boundary condition that $\mathscr{D}(\mathbf{r},\mathbf{r}')$ vanishes on the cavity surfaces. The only additional tool needed is the structure of the two-dimensional Coulomb Green's functions $\mathscr{G}^{(E,M)}(0;\boldsymbol{\rho},\boldsymbol{\rho}')$ which obey

$$-\nabla_\perp^2\mathscr{G}^{(E,M)}(0;\boldsymbol{\rho},\boldsymbol{\rho}')=\delta(\boldsymbol{\rho}-\boldsymbol{\rho}') \ , \tag{4.21}$$

with the boundary conditions that the magnetic function (M) vanishes on the circle of radius R while the normal gradient of the electric function (E) is constant on this circle. The familiar image technique yields

$$\mathscr{G}^{(E,M)}(0;\boldsymbol{\rho},\boldsymbol{\rho}') =-\frac{1}{2\pi}\left[\ln\left[\frac{\boldsymbol{\rho}^2-2\boldsymbol{\rho}\cdot\boldsymbol{\rho}'+\boldsymbol{\rho}'^2}{R^2}\right] \pm\ln\left[\frac{\boldsymbol{\rho}^2\boldsymbol{\rho}'^2-2\boldsymbol{\rho}\cdot\boldsymbol{\rho}'R^2+R^4}{R^4}\right]\right] . \tag{4.22}$$

With these results in hand, it is now a matter of straightforward, albeit tedious, algebra to verify that Eq. (4.3) does actually satisfy Eq. (3.1).

If the boundary correction terms were deleted from Eqs. (4.15) with the $F_{|m|}^{(E,M)}(\mu_n\rho)$ replaced by $K_{|m|}(\mu_n\rho)$, the radial Green's function (4.17) would become that of the cylindrical coordinate expansion of the parallel-plate problem solved in the preceeding section. Hence we discard the $K_{|m|}(\mu_n\rho)$ from the $F_{|m|}^{(E,M)}(\mu_n\rho)$ functions so as to obtain the alteration of the previous parallel-plate problem which is brought about by the presence of the conducting cylindrical wall. This obviates the necessity of removing the proper field contribution from the infinite sums in Eq. (4.5), which is a delicate task. We denote the remaining, cylindrical-wall contribution to the radial Green's functions by $\overline{\mathscr{G}}_m^{(E,M)}(\mu_n;\rho,\rho')$ and, correspondingly, to the radiation gauge Green's function by $\tilde{D}_{kl}(\omega;\mathbf{r},\mathbf{r}')$. [The first logarithm in Eq. (4.22) is also deleted in the construction of this function.] Thus the (complex) frequency shift for the parallel-plate problem given by Eq. (3.13) is now corrected by the cylindrical-wall addition to give the closed-cavity solution

$$\omega-\omega_c'=-\frac{i}{2}\gamma_c(\omega)+\omega[\Sigma_P(\omega)+\Sigma_S(\omega)] \ , \tag{4.23}$$

where

$$\Sigma_S(\omega)=-r_0\tilde{D}_{xx}(\omega;0,0) \ . \tag{4.24}$$

Referring to Eqs. (4.3) and (4.5), we see that $\tilde{D}_{xx}(\omega;0,0)$ involves $t(0)$ for the TE modes and $t'(0)$ for the TM modes. Hence we need only the trigonometric functions

$$t_E(k_nz)=\cos(k_nz) \tag{4.25a}$$

and

$$t_M(k_nz)=\sin(k_nz) \ . \tag{4.25b}$$

In either case, the boundary conditions of Eqs. (4.7) require that

$$k_n=(n+\tfrac{1}{2})\pi/L \ . \tag{4.26}$$

Again referring to Eq. (4.3), we see that the evaluation of $\tilde{D}_{xx}(\omega;0,0)$ entails only the linear terms in ρ and ρ' in $\overline{\mathscr{G}}_m^{(E,M)}(\mu_n;\rho,\rho')$. Since $I_{|m|}(\mu\rho)\sim\rho^{|m|}$, only $|m|=1$ contributes with, for small ρ,

$$I_1(\mu_n\rho)\simeq\tfrac{1}{2}\mu_n\rho \ . \tag{4.27}$$

The $m=\pm1$ sum in Eq. (4.13) coupled with this small-ρ behavior produces a factor of $\boldsymbol{\rho}\cdot\boldsymbol{\rho}'$ and it is now a matter of straightforward algebra to compute the result:

$$\Sigma_S(\omega)=-\frac{r_0}{L}\sum_{n=0}^{\infty}\left[\frac{K_1'(\mu_nR)}{I_1'(\mu_nR)}+\frac{k_n^2c^2}{\omega^2}\left[\frac{K_1(\mu_nR)}{I_1(\mu_nR)}-\frac{K_1(k_nR)}{I_1(k_nR)}\right]\right] . \tag{4.28}$$

Equation (4.28) is the major result of our work. We turn now to discuss some of its features. First we note that the sum of Eq. (4.28) converges very rapidly: For large n, $\mu_n\sim k_n\sim n\pi/L$ and we see that the sum is exponentially damped,

$$\frac{K_1'(\mu_nR)}{I_1'(\mu_nR)}\sim\frac{K_1(\mu_nR)}{I_1(\mu_nR)}\sim\pi e^{-2\pi nR/L} \ . \tag{4.29}$$

Next we note that, just as in the parallel-plate geometry, thresholds appear in the sum (4.28) at $\omega=k_Nc$, $N=0,1,2,\ldots$. Near the Nth threshold μ_N is very small. Using the small-argument limit of the Bessel functions one finds that

$$\left[\frac{K_1'(\mu_NR)}{I_1'(\mu_NR)}+\frac{K_1(\mu_NR)}{I_1(\mu_NR)}\right]\sim\ln\mu_N^2R^2, \quad \omega\sim k_Nc \tag{4.30}$$

which produces a logarithmic singularity,

$$\Sigma_S(\omega)\sim-\frac{r_0}{L}\ln(k_N^2-\omega^2/c^2)R^2, \quad \omega\sim k_Nc \ . \tag{4.31}$$

The frequency shift for the cavity [Eq. (4.23)] involves the sum of $\Sigma_S(\omega)$ and the previously calculated parallel-plate contribution $\Sigma_P(\omega)$, whose real part is given in Eq. (3.18). Looking back at Eq. (3.18), we see that the logarithmic divergence in $\Sigma_S(\omega)$ is exactly canceled by the logarithmic divergence in $\Sigma_P(\omega)$.

After passing the Nth threshold, one must make the replacement

$$\mu_N=-i\tilde{\mu}_N=-i(\omega^2/c^2-k_N^2)^{1/2} \ , \tag{4.32}$$

and the Bessel functions become

$$I_1(\mu_NR)=-iJ_1(\tilde{\mu}_NR) \tag{4.33a}$$

and

$$K_1(\mu_N R)=-\frac{\pi}{2}H_1^{(1)}(\tilde{\mu}_N R)$$
$$=-\frac{\pi}{2}[J_1(\tilde{\mu}_N R)+iN_1(\tilde{\mu}_N R)]\ . \tag{4.33b}$$

Thus, on passing the Nth threshold, we must write

$$\frac{K_1'(\mu_N R)}{I_1'(\mu_N R)}+\frac{k_N^2c^2}{\omega^2}\frac{K_1(\mu_N R)}{I_1(\mu_N R)}$$
$$=\frac{\pi}{2}\left[\frac{N_1'(\tilde{\mu}_N R)}{J_1'(\tilde{\mu}_N R)}+\frac{k_N^2c^2}{\omega^2}\frac{N_1(\tilde{\mu}_N R)}{J_1(\tilde{\mu}_N R)}\right]$$
$$-\frac{\pi i}{2}\left[1+\frac{(N+\frac{1}{2})^2\pi^2c^2}{\omega^2L^2}\right]. \tag{4.34}$$

Since this continuation must be performed on all the thresholds that lie lower than N, we see that the imaginary part of Eq. (4.28) gives

$$I_S(\omega)=-2\,\mathrm{Im}[\omega\Sigma_S(\omega)]$$
$$=-\pi\omega\frac{r_0}{L}\sum_{n=0}^{N}\left[1+\frac{(n+\frac{1}{2})^2\pi^2c^2}{\omega^2L^2}\right]. \tag{4.35}$$

The finite sums that appear here are well known, and it is easy to prove that the cylindrical side correction $I_S(\omega)$ exactly cancels the parallel-plate decay constant $I_P(\omega)$ which is given by Eq. (3.15). This, of course, must happen since we have no dissipation in our idealized cavity: There is a frequency shift in the cyclotron motion but no decay.

Finally, we note that there are poles in $\Sigma_S(\omega)$ when the frequency ω exceeds a threshold,

$$\Sigma(\omega)\simeq\frac{{}^{(E,M)}\lambda_{n,l}^2}{\omega^2-{}^{(E,M)}\omega_{n,l}^2}\ . \tag{4.36}$$

The frequencies ${}^{(E,M)}\omega_{n,l}$ are the eigenfrequencies of the TE and TM normal modes of the cavity labeled by the integers n,l. In view of Eq. (4.34), we see that we have poles corresponding to TE modes when $\tilde{\mu}_n R=\alpha_l$, where α_l are the roots determined by

$$J_1'(\alpha l)=0\ . \tag{4.37a}$$

These roots give the TE eigenfrequencies

$${}^{(E)}\omega_{n,l}^2=\left[k_n^2+\frac{\alpha_l^2}{R^2}\right]c^2\ . \tag{4.38a}$$

Expanding $J_1'(\tilde{\mu}_n R)$ about this root, one finds that the coupling of the mode is given by

$${}^{(E)}\lambda_{n,l}^2=-\pi\frac{r_0}{L}\frac{N_1'(\alpha_l)}{J_1''(\alpha_l)}\frac{\alpha_l c^2}{R^2}\ . \tag{4.39a}$$

Similarly, the TM mode eigenfrequencies are determined by

$$J_1(\beta_l)=0\ , \tag{4.37b}$$

with

$${}^{(M)}\omega_{n,l}^2=\left[k_n^2+\frac{\beta_l^2}{R^2}\right]c^2 \tag{4.38b}$$

and

$${}^{(M)}\lambda_{n,l}^2=-\pi\frac{r_0}{L}\frac{k_n^2c^2}{{}^{(M)}\omega_{n,l}^2}\frac{N_1(\beta_l)}{J_1'(\beta_l)}\frac{\beta_l c^2}{R^2}\ . \tag{4.39b}$$

Using the Wronskian and other familiar relations amongst Bessel functions, it is not difficult to prove that

$${}^{(E)}\lambda_{n,l}^2=\frac{r_0}{L}\frac{2c^2}{(\alpha_l^2-1)R^2}\frac{\alpha_l^2}{J_1(\alpha_l)^2}\ , \tag{4.40a}$$

and that

$${}^{(M)}\lambda_{n,l}^2=\frac{r_0}{L}\frac{k_n^2c^2}{{}^{(M)}\omega_{n,l}^2}\frac{2c^2}{R^2}\frac{1}{J_0(\beta_l)^2}\ , \tag{4.40b}$$

which show that these squared coupling constants are indeed positive. At first glance one might suppose that the complete result for the closed cavity is obtained by simply summing up all the TE and TM poles (4.36) as we illustrated before in formula (2.18). However, both ${}^{(E)}\lambda_{n,l}^2$ and ${}^{(M)}\lambda_{n,l}^2$ are proportional to l in the limit of large n and l while both ${}^{(E)}\omega_{n,l}^2$ and ${}^{(M)}\omega_{n,l}^2$ behave as $n^2/L^2+l^2/R^2$ in this limit. Hence the double sum over n and l does not converge but rather linearly diverges. This divergence reflects the fact that the proper field of the charged particle must be removed. This we have done unambiguously by expressing the frequency shift as the sum (4.23) of the shift for the parallel-plate problem, where the proper field was removed by deleting the no-image contribution, plus the rapidly convergent sum (4.28) that yields the correction resulting from the cylindrical cavity wall.

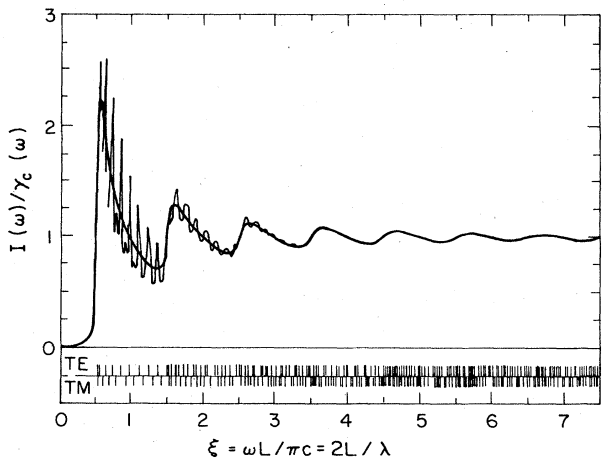

FIG. 7. Decay constant $I(\omega)/\gamma_c(\omega)$ given by Eq. (4.41) for a charged particle moving in a small orbit about the axis and centered in the midplane of a cylindrical cavity with $\delta/L=0.025$ corresponding to $Q=20$ and an aspect ratio $R/L=7$ (thin line). This is to be compared to the decay constant for the parallel-plate limit (3.22) with $\delta/L=0.025$ (thick line). Frequency is measured in units of $\xi=\omega L/\pi c=2L/\lambda$ which is the number of wavelengths that fit between the flat endcaps of the cavity.

B. Results

Having now described the physical and mathematical structure of our result, let us turn to its numerical consequences. As we have discussed before, the effect of the cavity dissipation can be modeled by replacing the real frequency ω by the complex extension $\omega+i\Gamma/2$. Thus we numerically compute

$$\omega-\omega_c' = -\frac{i}{2}I(\omega)+R(\omega)$$
$$= -\frac{i}{2}\gamma_c(\omega)+\omega[\Sigma_P(\omega+i\Gamma/2)+\Sigma_S(\omega+i\Gamma/2)] , \tag{4.41}$$

where $\Sigma_P(\omega+i\Gamma/2)$ is obtained from Eq. (3.21) and $\Sigma_S(\omega+i\Gamma/2)$ is obtained from Eq. (4.28). As we remarked before, the sum defining $\Sigma_S(\omega)$ converges very rapidly [cf. Eq. (4.29)] and so this numerical evaluation is not difficult having in memory proper routines for the Bessel functions.[14]

As a check on the calculation, we first plot the decay constant and frequency shift for a cavity with a large radius-to-height ratio, $R/L=7$, which should be close to the simple parallel-plate limit. We do this for a rather lossy case, $\Gamma=\omega/Q$, with $Q=20$, so that the cavity mode structure is smoothed. Just as in the parallel-plate case, it is convenient to measure the cyclotron frequency in terms of the dimensionless variable $\xi=\omega L/\pi c=2L/\lambda$ which is the (fractional) number of wavelengths that fit between the two flat endcaps. The decay constant is compared to the parallel-plate limit in Fig. 7 and the frequency shift is compared to the parallel-plate limit in Fig. 8. We see that the limit is indeed approached for higher frequencies.

Having made this check, we now turn to exhibit the results for the Penning trap with cylindrical geometry.[6] It has the aspect ratio $R/L=1.186$. So as to exhibit the general features of our result, we first choose a low quality factor $Q=50$ and examine a large range $0<\xi<7.5$. The decay constant $I(\omega)$ is plotted in Fig. 9. At lower

TABLE I. Cavity mode structure for $R/L=1.186$.

$\xi=2L/\lambda$	n	l	$Q\delta/L$	$\lambda_{n,l}^2R^2L/2r_0c^2$
		TE modes		
3.535	3	1	0.7414	4.189
3.781	3	2	0.9976	8.651
4.017	2	4	1.116	18.51
4.022	0	5	1.181	23.44
4.183	3	3	1.047	13.57
4.263	1	5	1.167	23.44
		TM modes		
3.611	0	4	0.5425	0.4022
3.648	3	1	0.5425	5.675
3.702	2	3	0.5425	7.314
3.878	1	4	0.5425	3.138
3.974	3	2	0.5425	8.611
4.363	2	4	0.5425	6.885
4.439	3	3	0.5425	9.970
4.449	0	5	0.5425	0.3273

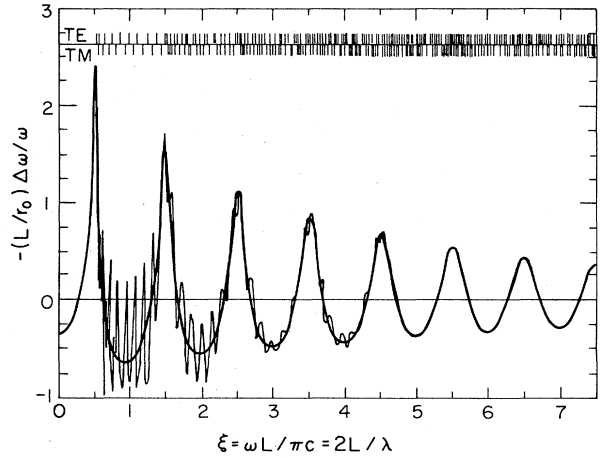

FIG. 8. Fractional frequency shifts corresponding to the decay constants plotted in Fig. 7.

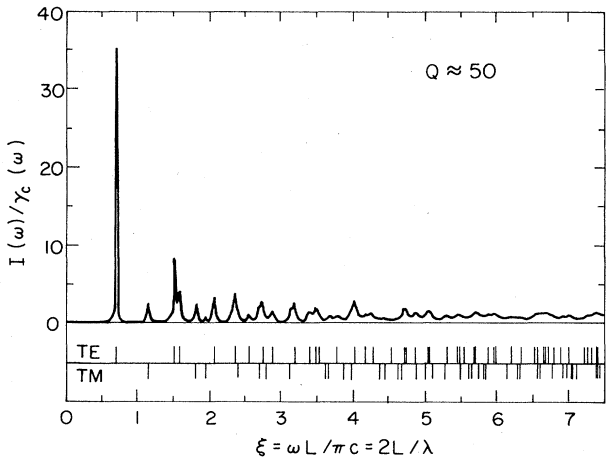

FIG. 9. Decay constant $I(\omega)/\gamma_c(\omega)$ for a charged particle moving in a small orbit about the axis and centered in the midplane of a cylindrical cavity with $Q=50$ and an aspect ratio $R/L=1.186$. The ticks place the TE and TM cavity mode frequencies.

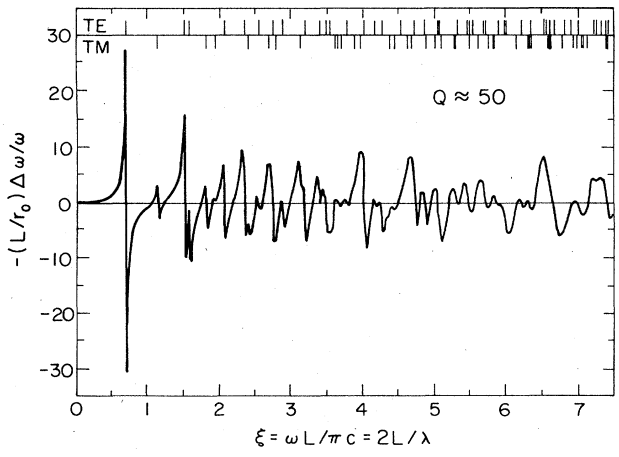

FIG. 10 Fractional frequency shift in the cylindrical cavity of Fig. 9.

frequencies it has distinct peaks corresponding to the cavity normal modes, but these merge as the frequency increases into the region where the mode spacing is less than the cavity width. At large frequencies, $I(\omega)$ approaches the free-space value $\gamma_c(\omega)$. The frequency shift $R(\omega)$ is shown in Fig. 10. There are dispersive structures in the low-frequency region that correspond to the absorptive peaks in Fig. 9, but as the frequency increases these structures become less distinct.

Experiments are generally performed in the region $3.5<\xi<4.5$, and we turn now to examine the nature of our result in this region in detail. But before passing to this, it is instructive to first note the mode structure in this interval which is displayed in Table I. These are the cavity modes which couple to the cyclotron motion at the center of the cavity, the modes with a nonvanishing electric field at the center which is perpendicular to the cylinder axis. The mode frequencies and coupling constants given in the table are determined from Eqs. (4.37), (4.38), and (4.40), while the quality factors for the various modes follow from the formulas[15]

$$\frac{1}{{}^{(E)}Q_{n,l}}=\frac{\delta}{R}\left[\frac{\alpha_l^2}{\alpha_l^2-1}+\frac{k_n^2c^2}{\omega_{n,l}^2}\left[\frac{R}{L}-1\right]\right] \tag{4.42a}$$

and

$$\frac{1}{{}^{(M)}Q_{n,l}}=\frac{\delta}{R}\left[1+\frac{R}{L}\right], \tag{4.42b}$$

where δ is the skin depth of the conducting surface. From the table we see that, on average, ${}^{(E)}Q\approx 2\,{}^{(M)}Q$, with

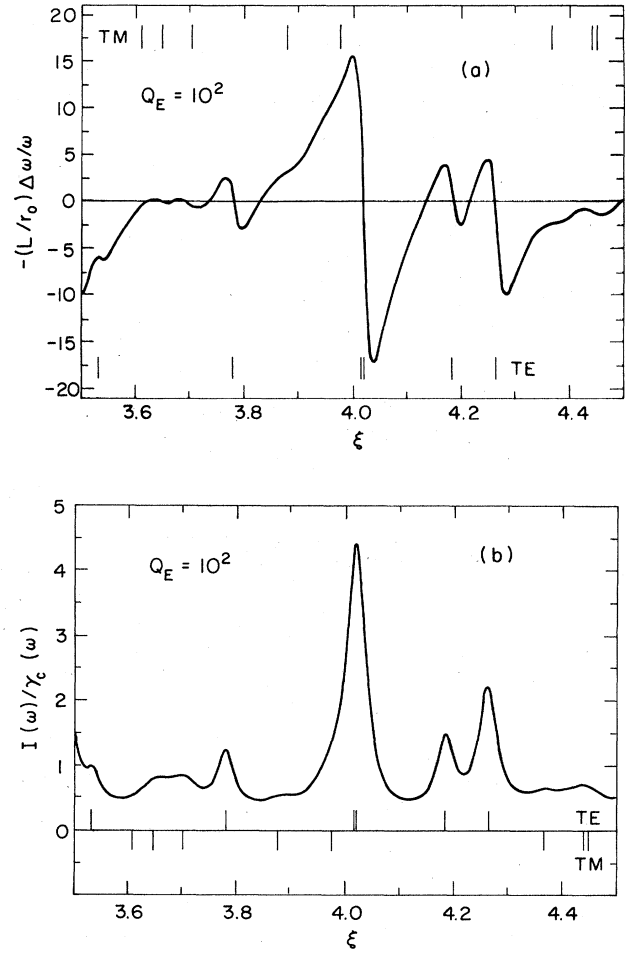

FIG. 11. Cavity effects for $R/L=1.186$ and ${}^{(E)}Q=100$. (a) Frequency shift. (b) Decay constant.

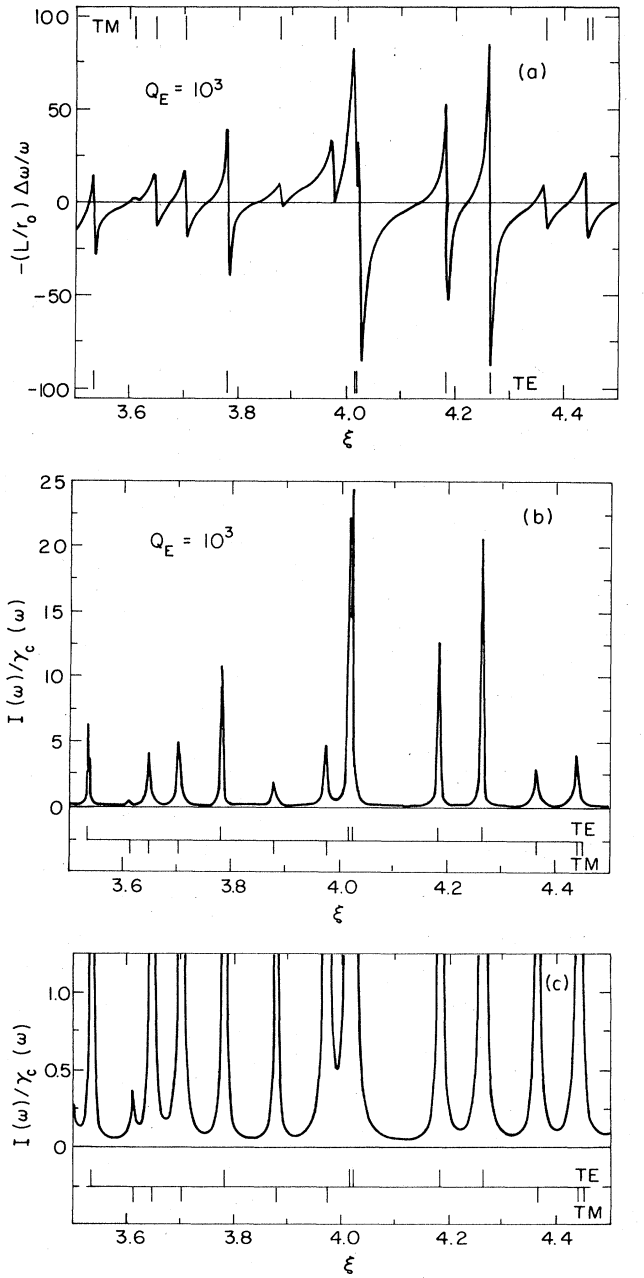

FIG. 12. Cavity effects for $R/L=1.186$ and ${}^{(E)}Q=1000$. (a) Frequency shift. (b) Decay constant. (c) Magnified section of the smaller values of the decay constant.

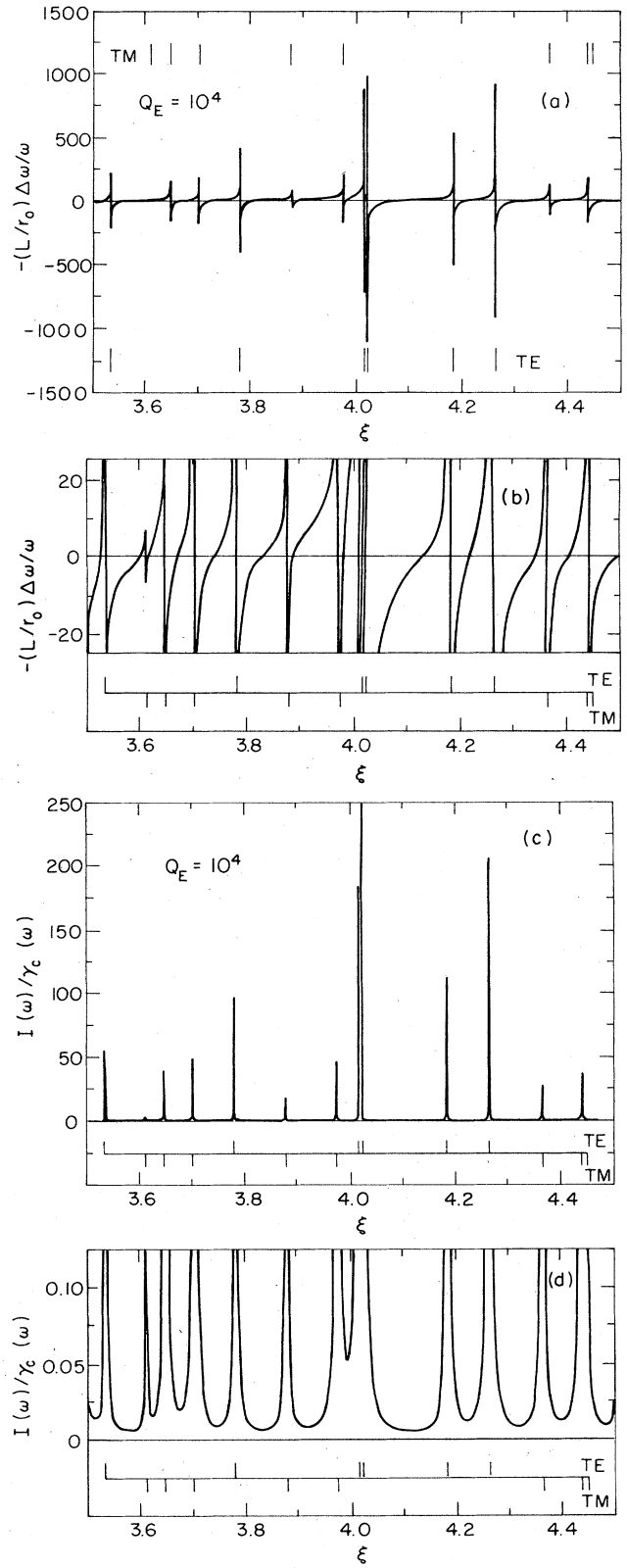

FIG. 13. Cavity effects for $R/L = 1.186$ and ${}^{(E)}Q = 10000$. (a) Frequency shift. (b) Magnified section of the smaller values of the frequency shift. (c) Decay constant. (d) Magnified section of the smaller values of the decay constant.

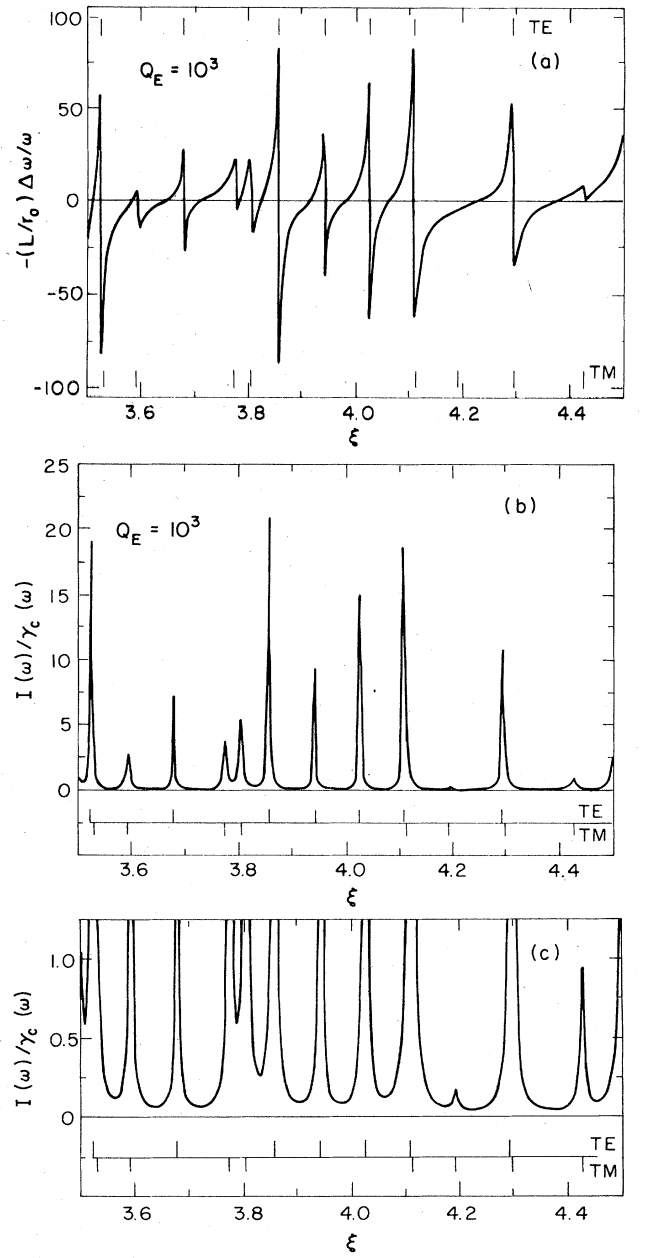

FIG. 14. Cavity effects with $R/L = 1.5$ and ${}^{(E)}Q = 1000$ for the frequency range of an experiment that employs a larger trap size. (a) Frequency shift. (b) Decay constant. (c) Magnified section of the smaller values of the decay constant.

the deviations from this average being less than 10% (except for a TE mode that has a very small coupling). We approximately account for this difference in cavity widths by using the complex frequency $\omega(1+i/2\,{}^{(E)}Q)$ in the TE denominator function $I_1'(\mu_n R)$ in Eq. (4.28) while all the other complex frequencies are given by $\omega(1+i/2\,{}^{(M)}Q)$, with ${}^{(M)}Q = {}^{(E)}Q/2$. [By keeping all the other complex frequencies the same, the threshold cancellation discussed after Eq. (4.31) is preserved, as it must be.] The quality-factor formulas (4.42) apply to an ideal cylindrical cavity

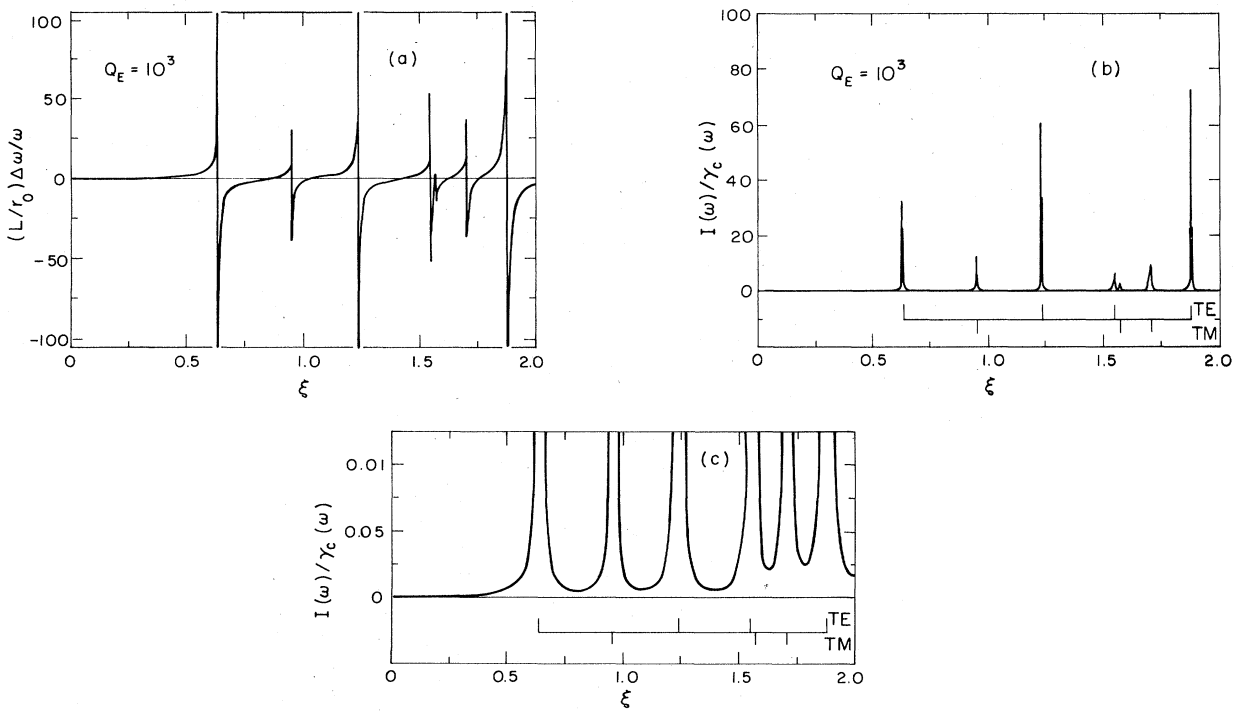

FIG. 15. Cavity effects with $R/L=1.5$ and ${}^{(E)}Q=1000$ for the frequency range of an experiment that employs a smaller trap size. (a) Frequency shift. (b) Decay constant. (c) Magnified section of the smaller values of the decay constant.

with perfect geometry. Actual cylindrical Penning traps contain holes and slits, and their quality factors are difficult to calculate accurately. Thus, although one could alter the individual modes in the interval $3.5<\xi<4.5$ by putting in the exact widths of Eqs. (4.42), this is not warranted by the uncertainty in our knowledge of the widths of the experimental traps. Thus, we use the simple substitution described above to compute the decay constants and frequency shifts plotted in Figs 11, 12, and 13 for ${}^{(E)}Q=100$, 1000, and 10 000. As the quality factor Q increases, the mode structure becomes, of course, more prominent. At higher Q the decay constant is sharply peaked at the resonant mode frequencies, with, for example $I(\omega)$ varying from $0.06\gamma_c(\omega)$ to $24\gamma_c(\omega)$ when ${}^{(E)}Q=1000$.

To set the scale for the frequency shifts, we note that in the experimental traps $r_0/L\approx 8\times 10^{-13}$, while, as discussed in Sec. I, the current experimental precision in the $g-2$ measurement is equivalent to a shift in the cyclotron frequency given by $\Delta\omega_c/\omega_c\approx 5\times 10^{-12}$. We see from the figures that, on this scale, very large shifts occur in the vicinity of the normal mode frequencies. For example, with ${}^{(E)}Q=1000$, one can have shifts as large as $\Delta\omega_c/\omega_c\approx 70\times 10^{-12}$, although for the most part the shifts are on the order of $\Delta\omega_c/\omega_c\approx 8\times 10^{-12}$. The presently employed Penning traps have a ring-to-endcap distance ratio of $\sqrt{2}$. To model this, we plot in Figs. 14 and 15 the cavity shifts for a cylindrical cavity with the aspect ratio $R/L=1.5$, again with ${}^{(E)}Q=1000$ and ${}^{(M)}Q=500$. Although the mode structure is slightly different, the shifts are about the same size as those in the cavity with the $R/L=1.186$ aspect ratio. In view of the uncertainties in the theoretical value of the anomaly discussed in Sec. I, a frequency shift as large as $\Delta\omega_c/\omega_c=140\times 10^{-12}$ would not be revealed by comparing the experimental and theoretical results for the anomaly. We conclude that an experimental search of this systematic effect should be made to confirm the present value of the g factor of the electron.

ACKNOWLEDGMENTS

This work was supported in part by the U. S. Department of Energy under Contract DE-AC06-81ER40048, by a grant from the National Science Foundation, and by research support from the University of Washington Graduate School.

[1]E. M. Purcell, Phys. Rev. **69**, 681 (1946).

[2]D. Kleppner, Phys. Rev. Lett. **47**, 233 (1981). Very recently, the inhibition of the radiation of a Rydberg atom between closely spaced plates was observed by R. Hulet, E. S. Hilfer, and D. Kleppner (unpublished).

[3]G. Gabrielse and H. G. Dehmelt, Phys. Rev. Lett. **55**, 67 (1985). Cavitylike effects on the radiation of a molecule separated from a single conducting plate by a thin dielectric layer have been observed by K. H. Drexhage, M. Fleck, H. Kuhn, F. P. Schafer, and W. Sperling, Ber. Bunsenges. Phys.

Chem. **70**, 1179 (1966). This experiment is also discussed by K. H. Drexhage, in *Progress in Optics,* edited by E. Wolf (North-Holland, Amsterdam, 1974), Vol. XII, p. 165. A variety of theoretical techniques have been used to study the radiation of an atom near a plate or between plates: H. Morawitz, Phys. Rev. **187**, 1792 (1969); H. Kuhn, J. Chem. Phys. **53**, 101 (1970); P. Stehle, Phys. Rev. A **2**, 102 (1970); M. R. Philpott, Chem. Phys. Lett. **19**, 435 (1973); P. W. Milonni and P. L. Knight, Opt. Commun. **9**, 119 (1973); R. R. Chance, A. Prock, and R. Silbey, J. Chem. Phys. **62**, 771 (1975).

[4]R. S. Van Dyck, Jr., P. B. Schwinberg, and H. G. Dehmelt, in *Atomic Physics 9,* edited by R. S. Van Dyck and E. N. Fortson (World Scientific, Singapore, 1984). [A review of this work is given by R. S. Van Dyck, Jr., P. B. Schwinberg, and H. G. Dehmelt, in *New Frontiers in High Energy Physics,* edited by B. Kursonoglu, A. Perlmutter, and L. Scott (Plenum, New York, 1978). An elementary account appears in P. Ekstrom and D. Wineland, Sci. Am. **243**, 105 (1980). An exhaustive account of the theory of the experiment is given by L. S. Brown and G. Gabrielse, Rev. Mod. Phys. (to be published)].

[5]D. G. Boulware, L. S. Brown, and T. Lee, Phys. Rev. D **32**, 729 (1985); D. G. Boulware and L. S. Brown, Phys. Rev. Lett. **55**, 133 (1985).

[6]G. Gabrielse and F. C. MacKintosh, Int. J. Mass Spectrom. Ion Phys. **57**, 1 (1984), explain the electrostatics of a cylindrical trap; such a trap is now being tested by G. Gabrielse and K. Helmerson.

[7]T. Kinoshita and J. Sapirstein, in *Atomic Physics 9,* edited by R. S. Van Dyck and E. N. Fortson (World Scientific, Singapore, 1984).

[8]E. Fischbach and N. Nakagawa, Phys. Rev. D **30**, 2356 (1984); Phys. Lett. **149B**, 504 (1984).

[9]K. Svozil, Phys. Rev. Lett. **54**, 742 (1985).

[10]L. S. Brown, G. Gabrielse, K. Helmerson, and J. Tan, Phys. Rev. Lett. **55**, 44 (1985).

[11]D. J. Wineland and H. Dehmelt, J. Appl. Phys. **46**, 919 (1975).

[12]For the Penning trap with a quadrupole electrostatic potential, $\omega_c' = [\omega_c + (\omega_c^2 - 2\omega_z^2)^{1/2}]/2$, where ω_z is the frequency of the axial oscillation.

[13]This has been noted before, for example, by L. S. Brown and G. J. Maclay, Phys. Rev. **184**, 1272 (1969), who used such a construction to derive the Casimir force between two conducting planes.

[14]The numerical computations were carried out on a VAX 11/780 using the MMBZIN code of the IMSL Library Reference Manual Edition 9, 1982, Vol. 3 for $I_0(z)$ and $I_1(z)$ and the code for $K_0(z)$ and $K_1(z)$ given by K. H. Burrel, Algorithm 484 in Collected Algorithms from CACM. We thank W. Petersen for bringing this latter useful algorithm to our attention.

[15]See, for example, R. Beringer, in *Technique Of Microwave Measurements,* Vol. 11 of *MIT Radiation Laboratory Series,* edited by C. G. Montgomery (McGraw-Hill, New York, 1947), pp. 297–301. We should note that the quality factor Q for the TM modes in an experimental cavity may be considerably smaller because of slits in the cavity that inhibit current flows in some directions.